https://doi.org/10.5194/egusphere-2026-6894
Preprint. Discussion started: 12 November 2026
© Author(s) 2026. CC BY 4.0 License.

Improved Daily Fertilizer-Induced Ammonia Emission Inventory for China by Combining Satellite Remote Sensing and Machine Learning

Yunkai Yang[1], Baojie Li[1], Weimeng Zhang[1], Yongqi Zhao[2], Junjie Liu[1], Wanglijing Gu[1], Hong Liao[1]

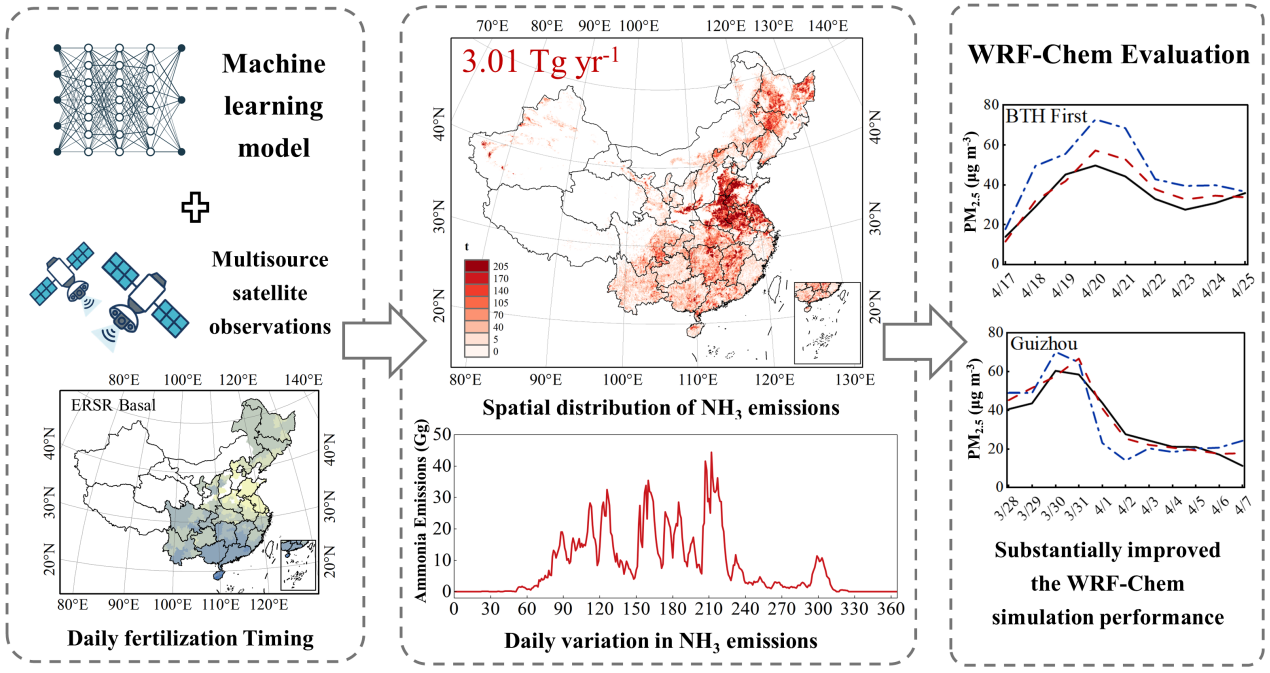
[1]Collaborative Innovation Center of Atmospheric Environment and Equipment Technology, Jiangsu Key Laboratory of Atmospheric Environment Monitoring and Pollution Control, School of Environmental Science and Engineering, Nanjing University of Information Science & Technology, Nanjing 210044, China
[2]State Key Laboratory of Atmospheric Environment and Extreme Meteorology, Institute of Atmospheric Physics, Chinese Academy of Sciences, Beijing 100029, China

Correspondence to: Baojie Li (baojieli@nuist.edu.cn)

Hong Liao (hongliao@nuist.edu.cn)

Abstract. Temporal variability of fine particulate matter ($PM_{2.5}$) pollution is strongly influenced by ammonia (NH_3) emissions, particularly their high-frequency variation driven by nitrogen fertilization. However, the unavailability of daily fertilization dates renders the spatiotemporal distribution of fertilizer-induced NH_3 emissions unclear, thereby limiting the accuracy of NH_3 emission estimates and $PM_{2.5}$ prediction. We developed a new method that identifies daily fertilization dates from multisource satellite observations and quantifies daily NH_3 emissions using machine learning. The identified fertilization dates correlated well with reported fertilization dates (mean correlation coefficient R = 0.96). Total NH_3 emissions from major crop fertilization were estimated at 3.01 Tg in 2021. The 10% of days with the highest emissions accounted for 33.11% of the annual total, with an average of 31.15 Gg d^{-1} on these days. The new inventory substantially improved the Weather Research and Forecasting model coupled with Chemistry (WRF-Chem) simulation of $PM_{2.5}$, reducing the average root mean square error (RMSE) by 35.34% during typical fertilization events. These daily datasets enable a shift from annual emission controls to temporally targeted mitigation strategies, and suggest that optimizing fertilization timing could mitigate severe $PM_{2.5}$ pollution.

https://doi.org/10.5194/egusphere-2026-6894
Preprint. Discussion started: 12 November 2026
© Author(s) 2026. CC BY 4.0 License.



Graphical abstract

1 Introduction

Fine particulate matter ($PM_{2.5}$) is strongly influenced by NH_3, the predominant alkaline gas in the atmosphere (Qiao et al., 2018). By neutralizing sulfuric and nitric acids formed from SO_2 and NO_x, NH_3 promotes secondary inorganic aerosol (SIA) formation and exacerbates regional $PM_{2.5}$ air pollution (Xu et al., 2019; Fowler et al., 2013). Excess NH_3 deposition also causes ecological damage, including aquatic eutrophication, soil acidification, and biodiversity loss (Chen et al., 2023; Zhan et al., 2017). Although China has improved air quality through stringent end-of-pipe controls on SO_2 and NO_x emissions (Zhang et al., 2019), this strategy is constrained by increasing marginal abatement costs (Li et al., 2025; Geng et al., 2021). By contrast, NH_3 emissions in China remain largely unregulated, and national emissions now exceed those from Europe and the United States combined (Liu et al., 2022a). Nitrogen fertilizer application is the dominant NH_3 source in China, accounting for approximately 40% of national emissions in recent years (Li et al., 2021; Li et al., 2024; Shen et al., 2026) and its daily emission variability strongly influences $PM_{2.5}$ pollution.

The formation of SIA is strongly influenced by the temporal dynamics of NH_3 emissions (Ren et al., 2025a; Wang et al., 2021b). Fertilizer application is the main cause of daily variations in these emissions. It releases large amounts of NH_3 within a short period, which can rapidly increase regional $PM_{2.5}$ concentrations (Kuang et al., 2020). NH_3 emissions from fertilizer typically peak between 24 and 72 h after application and are strongly modulated by meteorological conditions, including

https://doi.org/10.5194/egusphere-2026-6894
Preprint. Discussion started: 12 November 2026
© Author(s) 2026. CC BY 4.0 License.

temperature and precipitation (Yang et al., 2020; Xu et al., 2021). Accurate simulation of daily NH_3 emission dynamics thus requires NH_3 emission inventories at daily resolution. However, most existing NH_3 emission inventories are compiled at monthly resolution (Kang et al., 2016; Zhang et al., 2018; Wang et al., 2021a). Such inventories may introduce systematic biases into air quality simulations.

In addition to their coarse temporal resolution, current emission inventories are constrained by the inherent limitations of traditional estimation methods and the variability of agricultural activities across regions and seasons. Most existing inventories are developed using the emission factor (EF) approach (Li et al., 2021; Huang et al., 2012), which applies temporally invariant EFs. Such static EFs fail to reflect the temporal dynamics of NH_3 emissions, introducing large uncertainties into the resulting inventories (Zhan et al., 2021; Zhou et al., 2016). Moreover, fertilization timing largely governs the temporal pattern of agricultural NH_3 emissions, yet it remains highly uncertain. To our knowledge, few studies have identified fertilization dates at a daily resolution with high accuracy. The few daily inventories currently available account only for daily meteorological variability, with fertilization timing still prescribed by static crop calendars (Ren et al., 2023; Ye et al., 2022).

Satellite observations from the Infrared Atmospheric Sounding Interferometer (IASI) and the Cross-track Infrared Sounder (CrIS), acquired during their daytime overpasses, enable the identification of fertilization dates at daily resolution by detecting abrupt increases in NH_3 column densities following fertilization events (Ding et al., 2024; Chen et al., 2025; Xia et al., 2025). In parallel, advances in machine learning offer the potential to overcome the limitations of static EFs. A hybrid bidirectional long short-term memory-random forest (BiLSTM-RF) model combines the ability of BiLSTM to capture temporal dependencies and continuous nonlinear relationships with the robust generalization of RF under limited sample sizes, thereby avoiding both the prediction discontinuities of tree-based models and the overfitting of deep learning models trained on small datasets. This hybrid model has been shown to outperform conventional machine learning models at the daily scale (Yin et al., 2020).

In this study, we integrated daily NH_3 column retrievals from the IASI and the CrIS with crop phenology data to develop a method for identifying crop-specific fertilization dates and their associated uncertainties across China. We then used a machine learning algorithm (BiLSTM-RF) trained on 4,589 field NH_3 emission measurements to construct a daily NH_3 emission inventory at 5-arcminute spatial resolution from fertilizer application for rice, wheat, and maize for China in 2021. We evaluated the accuracy of the inventory using the Weather Research and Forecasting model coupled with Chemistry (WRF-Chem). These daily datasets enable a shift from annual emission controls to temporally targeted interventions, and suggest that optimizing fertilization timing could mitigate severe $PM_{2.5}$ pollution.

https://doi.org/10.5194/egusphere-2026-6894
Preprint. Discussion started: 12 November 2026
© Author(s) 2026. CC BY 4.0 License.

2 Data and Methods

2.1 Fertilization Timing Identification Using Remote Sensing

To identify fertilization dates, phenological stages corresponding to basal and topdressing fertilization events were identified from a high-resolution crop phenology dataset for the three major crops (rice, wheat, and maize) in China (Luo et al., 2020). These stages defined preliminary fertilization time windows for each prefecture-level city (Zhao et al., 2023). The windows were then refined against daily atmospheric NH_3 column retrievals from IASI and CrIS, using the characteristic temporal pattern of NH_3 emission peaks following fertilizer application as the validation criterion (Yang et al., 2020; Xu et al., 2021). For each satellite, a search window W spanning ±7 days around the empirical fertilization date was defined, within which the enhancement ratio on day t was defined as:

$$\delta_S(t) = \frac{C_S(t)}{\bar{C}_S}, S \in \{IASI, CrIS\} \quad (1)$$

where $C_S(t)$ is the NH_3 column amount retrieved by satellite S on day t, and $\bar{C}_S$ is the mean column amount over window W. If the maximum enhancement ratio within W exceeded the defined threshold, the day immediately preceding this peak was designated as the final fertilization date. Otherwise, the empirical date T_{exp} was retained:

$$T = \begin{cases} t_S^* - 1, if\ \max(\delta_{IASI}, \delta_{CrIS}) \geq 1.4 \\ T_{exp}, otherwise \end{cases} \quad (2)$$

where t_S^* is the day within W at which the enhancement ratio reaches its maximum, δ_{IASI} and δ_{CrIS} are the enhancement ratios from IASI and CrIS, respectively. T_{exp} is the fertilization date derived from phenological data. Daily IASI NH_3 column retrievals were obtained from the NH3R-ERA5 reanalysis product (https://iasi.aeris-data.fr/), derived from MetOp-B and MetOp-C observations. Only daytime overpasses were used, as these are generally considered more sensitive to NH_3 column variability than nighttime overpasses (Liu et al., 2022b; Van Damme et al., 2014). Daily CrIS NH_3 column retrievals were obtained from the v1.6.4 retrieval product developed by the AER team (Shephard et al., 2020), derived from NOAA-20 (JPSS-1) observations. For both satellite datasets, only retrievals that passed the quality flags provided in the respective data products and had positive column amounts were retained.

2.2 Machine Learning Estimation of Daily NH_3 Emissions

2.2.1 Dataset Construction

The China National Knowledge Infrastructure (CNKI) and Web of Science (WoS) databases were systematically searched to construct a dataset of NH_3 emissions from cropland for model training. The following keywords were used in both database searches: (ammonia OR NH_3 OR "reactive nitrogen") AND (emission*) AND (fertilizer* OR fertiliser*) AND (China). Studies published between 2007 and 2022 were screened against the following five criteria: (1) field experiments only, with greenhouse and pot experiments excluded; (2) NH_3 emission monitoring spanning the complete crop growing season; (3) daily NH_3 emission measurements for at least 7 consecutive days following fertilization; (4) detailed documentation of

https://doi.org/10.5194/egusphere-2026-6894
Preprint. Discussion started: 12 November 2026
© Author(s) 2026. CC BY 4.0 License.

experimental site characteristics, meteorological conditions, soil properties, and field management practices; and (5) experimental crops restricted to rice, wheat, or maize. A total of 4,589 daily NH_3 emission records from 76 experimental sites were retained after screening (Table S1). For each record, ancillary data were extracted from the source publications (see Text S1.1). Meteorological and soil parameters not reported therein were supplemented from the Harmonized World Soil Database v2.0 (HWSD v2.0, https://gaez.fao.org/pages/hwsd) and the ERA5 reanalysis dataset from the European Centre for Medium-Range Weather Forecasts (https://cds.climate.copernicus.eu/datasets) The full dataset included NH_3 emissions from rice, wheat, and maize across China (excluding Hong Kong, Macao, and Taiwan). Dataset features were then preprocessed to standardize model inputs (see Text S1.2), and the dataset was randomly partitioned into a training set (80%), a validation set (10%) for hyperparameter tuning, and a test set (10%) for final model evaluation.

The prediction dataset was assembled using the same input features as the training set. Gridded spatial distributions of the three crops at a 5-arcminute resolution were derived from planting area statistics in the 2021 China Statistical Yearbook (NBS, 2022), following the spatial allocation method of Li et al (2021). Grid-level soil parameters were obtained from HWSD v2.0. Fertilizer application rates were taken from the 2021 National Agricultural Product Cost and Income Data Compilation (NDRC, 2022) and converted to N application rates using the N content and national usage proportion of each fertilizer type (urea, ammonium bicarbonate, compound fertilizer, and other forms). The proportions of basal and topdressing applications by region were determined from farmer survey data (Table S2). Three fertilization events were defined for each crop, namely basal application, first topdressing, and second topdressing. Daily meteorological variables for 7 consecutive days following each fertilization event were extracted from the ECMWF ERA5 reanalysis dataset.

2.2.2 Model Training and Evaluation

To capture the nonlinear relationships between cropland NH_3 emissions and their controlling factors (meteorological conditions, soil properties, and field management practices), we employed the BiLSTM-RF algorithm, which integrates two sub-models with complementary strengths. BiLSTM was adopted because its bidirectional gated architecture captures intrinsic dependencies among input features and learns continuous, high-dimensional nonlinear mappings. This avoids the prediction discontinuities caused by the discrete splits of traditional tree-based models (Wu et al., 2023; Joseph et al., 2023). RF was trained using a bootstrap ensemble strategy that aggregated predictions from multiple decision trees, enabling robust generalization under limited sample sizes (Miinalainen et al., 2023; Lyu et al., 2022; Ren et al., 2025b). Model-specific weight coefficients were then computed based on the mean relative error of each sub-model on the validation set (see Text S1.3), yielding the prediction:

$$\hat{y} = \omega_{BiLSTM} \cdot \hat{y}_{BiLSTM} + \omega_{RF} \cdot \hat{y}_{RF} \quad (3)$$

where ω_{BiLSTM} and ω_{RF} are the weights assigned to the BiLSTM and RF sub-models, $\hat{y}_{BiLSTM}$ and $\hat{y}_{RF}$ are their respective predictions, and $\hat{y}$ is the combined predicted output.

We further compared BiLSTM-RF with five commonly used algorithms, including multiple linear regression (MLR), generalized additive model (GAM), long short-term memory (LSTM) neural network, least squares boosting (LSBoost), and

https://doi.org/10.5194/egusphere-2026-6894
Preprint. Discussion started: 12 November 2026
© Author(s) 2026. CC BY 4.0 License.

extreme gradient boosting (XGBoost). Based on root mean square error (RMSE) and the coefficient of determination (R^2), BiLSTM-RF outperformed all alternative algorithms (Table S3).

All algorithms were implemented in MATLAB R2024a. The BiLSTM model was constructed using the Deep Learning Toolbox, with network layers defined using bilstmLayer and model training performed using trainNetwork. The RF model was built using TreeBagger, with the random seed fixed at a value of 1 to ensure reproducibility. Hyperparameters were optimized using the THRO algorithm (Wang et al., 2025b; see Text S1.4). The predictive accuracy of the BiLSTM-RF model was then evaluated on an independent test set (see Text S2.1 and Fig. S1a), and the relative importance of individual input variables in the BiLSTM-RF model was assessed using the feature importance scores provided by the RF sub-model (see Text S1.5 and Fig. S1b).

2.3 Accuracy and Uncertainty of Fertilization Timing

To evaluate the accuracy of the identified fertilization date dataset, reference dates were compiled from online agricultural news reports for major cities in the principal producing provinces of each crop (maize, wheat, and rice), yielding 479 valid samples (Table S4). Because few topdressing dates were reported for any individual crop, topdressing samples were pooled across the three crops, whereas basal fertilization data were evaluated crop by crop. All dates were converted to Julian day before analysis (i.e., the sequential day of the calendar year, with January 1 = 1). Identified dates were then compared with reported dates, and agreement was assessed using the Pearson correlation coefficient (R) and the mean bias, defined as the reported minus the identified date (in days).

The uncertainty in the fertilization date dataset constructed in this study arose primarily from the parameter settings of the algorithm for identifying fertilization dates and spatiotemporal gaps in satellite remote sensing data. Uncertainty in fertilization dates was quantified by combining sensitivity analysis with Monte Carlo simulation. For city k, 15 parameter scenarios were constructed by combining three time windows (±3, ±7, and ±10 days centered on the baseline fertilization date) with five peak concentration thresholds (1.2, 1.3, 1.4, 1.5, and 1.6 times the mean concentration within the time window). From the fertilization dates $D_{k,n}(n = 1,2,\dots,15)$ derived under these 15 scenarios, the mean ($\bar{D}_k$) and standard deviation (σ_k) of the resulting distribution were computed. The fertilization date for city k in the nth Monte Carlo simulation, ${D_k}^{(n)}$, is given by:

$$ {D_k}^{(n)} = \bar{D}_k + \varepsilon_k^{para,(n)} + \varepsilon_k^{miss,(n)}, n = 1,2,\dots,10000 \quad (4) $$

where $\varepsilon_k^{para,(n)}$ denotes parameter uncertainty (normally distributed, $N(0, {\sigma_k}^2)$), and $\varepsilon_k^{miss,(n)}$ denotes uncertainty arising from spatiotemporal gaps in satellite remote sensing data (uniformly distributed, $U(-7,7)$). The 25th and 75th percentiles of the resulting Monte Carlo distribution were taken as the lower and upper bounds of the fertilization date uncertainty for each city.

https://doi.org/10.5194/egusphere-2026-6894
Preprint. Discussion started: 12 November 2026
© Author(s) 2026. CC BY 4.0 License.

2.4 Uncertainty Analysis and WRF-Chem Evaluation of the Daily Inventory

Uncertainty in BiLSTM-RF predictions is quantified using an interquartile range approach. The 25th and 75th percentiles of the relative errors on the independent validation set were used as error scaling factors and applied to all grid cells to construct uncertainty intervals for NH_3 emissions from each of the three major crops and their total.

WRF-Chem simulations were conducted to further evaluate the accuracy of the daily emission inventory. Emissions of anthropogenic pollutants other than NH_3 (e.g., SO_2 and NO_x) were obtained from the 2021 Multi-resolution Emission Inventory for China (MEIC, http://meicmodel.org/) at a spatial resolution of 0.25° × 0.25°. Agricultural NH_3 emissions for the model were prepared by combining our inventory with inventories for other crops and livestock (Liu et al., 2025; Zhang et al., 2025). The model was configured with two nested domains, with horizontal resolutions of 27 km for the outer domain and 9 km for the inner domain. In the BTH region, Jiangsu, Henan, and Guizhou, six $PM_{2.5}$ pollution episodes coinciding with fertilization events were identified. For these episodes, the outer domain covered most of China, whereas the inner domain covered the provinces for each episode. Details of the model configuration are provided in Text S1.6.

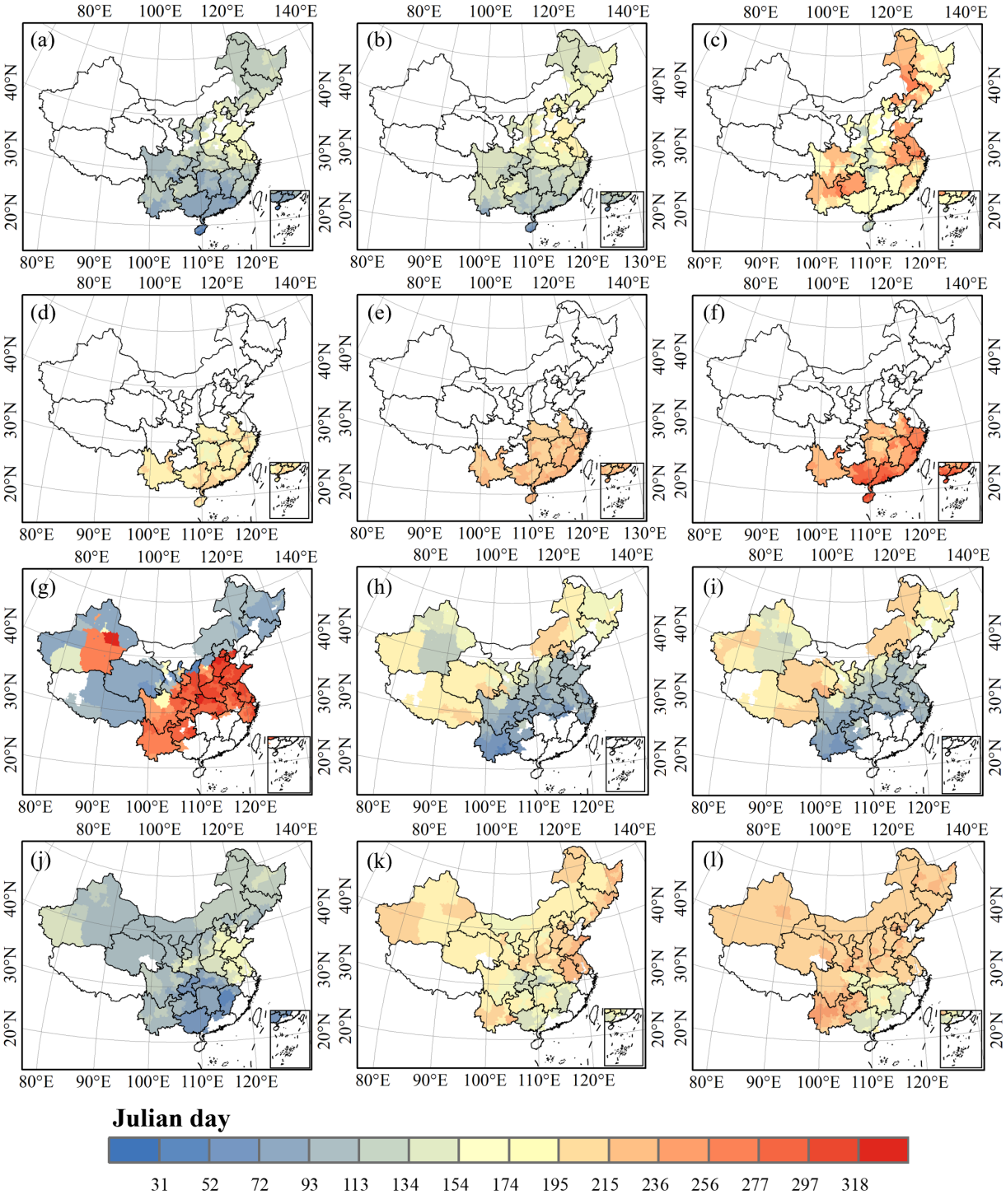
Two sets of simulations were conducted to assess the improvement in simulated $PM_{2.5}$ concentrations achieved using our inventory. Simulated $PM_{2.5}$ concentrations were evaluated against ground-based observations from the real-time air quality monitoring network of the China National Environmental Monitoring Centre (https://www.cnemc.cn/). Specifically, both simulations were evaluated during the pollution episodes using R and RMSE at all monitoring sites with complete data in the BTH region, Jiangsu, Henan, and Guizhou.

3 Results and Discussion

3.1 Fertilization Timing for Major Crops

We developed a dataset of fertilization dates for major crops in China at a daily resolution. The dataset integrated phenological observations with satellite remote sensing data and covered approximately 90% prefecture-level cities in China. The results reveal pronounced spatiotemporal heterogeneity in fertilization timing for all three major crops across China (Fig. 1). For any given crop, fertilization in southern regions generally preceded that in northern regions by 1–2 months, primarily due to marked climatic differences (Minoli et al., 2022; Wolkovich et al., 2012). Furthermore, the complex cropping systems in China, including winter and spring wheat as well as multi-season rice cultivation in the south (Qiu et al., 2025), resulted in a fertilization window extending from Julian day 24 to 338 in 2021. By contrast, previous studies have typically characterized fertilization timing at a monthly resolution and applied uniform fertilization windows across entire provinces (Wu et al., 2024; Huang et al., 2012), thereby overlooking substantial intra-provincial variation (Wu et al., 2021).

https://doi.org/10.5194/egusphere-2026-6894
Preprint. Discussion started: 12 November 2026
© Author(s) 2026. CC BY 4.0 License.



https://doi.org/10.5194/egusphere-2026-6894
Preprint. Discussion started: 12 November 2026
© Author(s) 2026. CC BY 4.0 License.

Figure 1: Spatial distribution of fertilization timing for major crops in China. Panel letters denote the fertilization stages for early and single-season rice (ERSR; a–c), late rice (LR; d–f), wheat (g–i), and maize (j–l), corresponding to basal application (left column), first topdressing (middle column), and second topdressing (right column).

The three major crops differ in their spatiotemporal fertilization patterns. Wheat fertilization was temporally concentrated, with basal application predominantly in October (43.82% of prefecture-level cities) and topdressing in spring (March to April, 59.36%). Rice fertilization exhibited a complex pattern. For late rice (LR), basal application was concentrated in July (65.73%), the first topdressing in August (81.82%), and the second topdressing in August (37.69%) and October (37.69%). For early and single-season rice (ERSR), basal application spanned April (24.91%) and May (34.16%). The first topdressing occurred primarily in May (28.93%) and June (39.64%). The second topdressing was distributed across June (35.71%) and August (21.43%). Maize fertilization exhibited a distinct latitudinal gradient in timing. Basal application was concentrated in April (33.67%), May (23.33%), and June (21.67%). The first topdressing occurred mainly in June (30.33%) and July (46.33%), and the second topdressing was primarily distributed in July (46.67%) and August (33.67%). Relative to the provincial uniform approach, these crop-specific patterns revealed intra-provincial differences in fertilization timing of up to several weeks, providing a robust empirical basis for developing emission inventories at high spatial resolution.

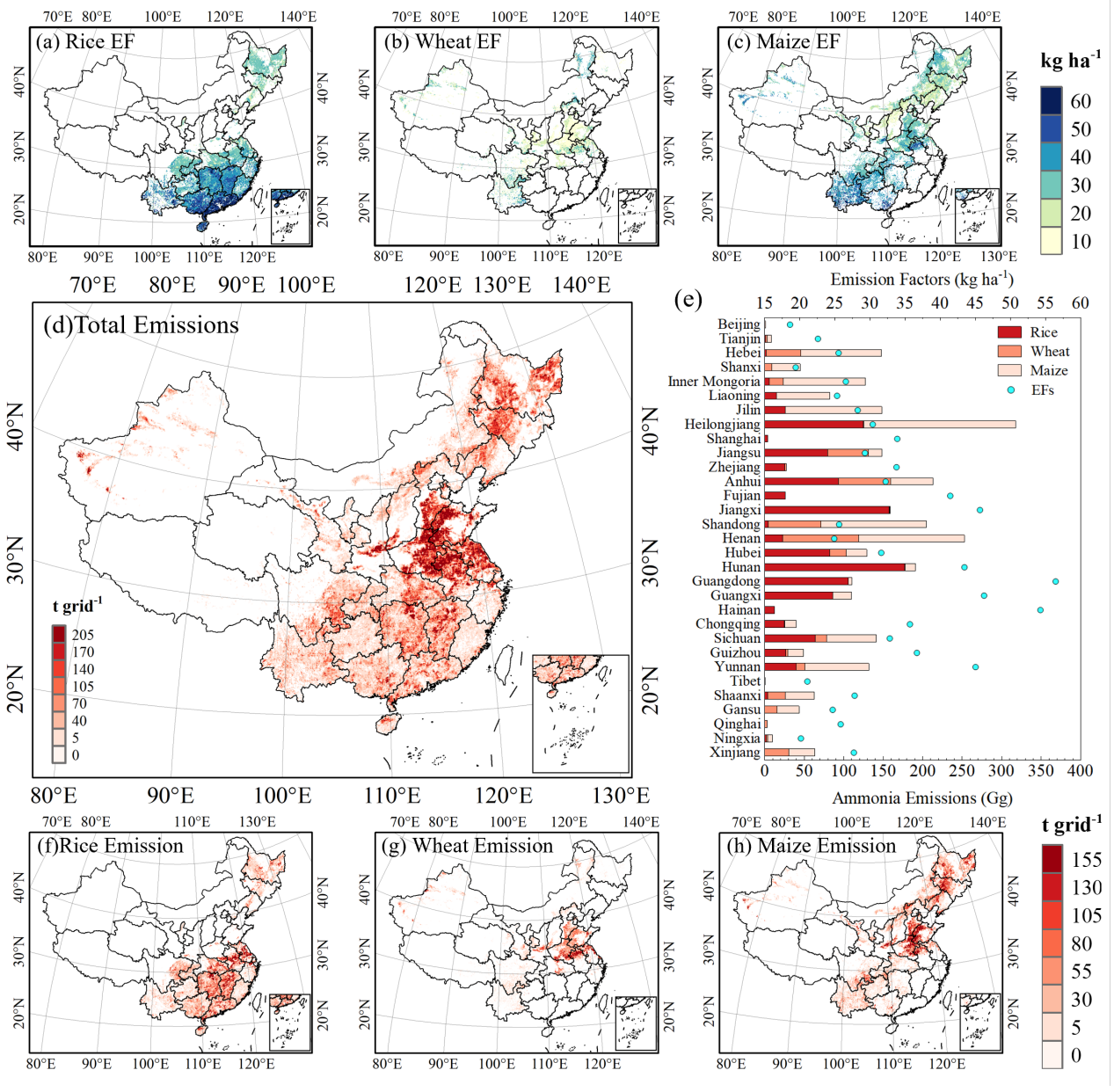
3.2 Spatial Distribution of NH_3 Emissions

Using a machine learning model, we derived daily high-resolution emission factors for major crops in China for 2021 (Fig. 2a–c). The national mean emission factor was 31.09 kg ha^{-1}, with crop-specific means of 40.48, 20.38, and 30.44 kg ha^{-1} for rice, wheat, and maize, respectively. By integrating these emission factors with gridded planted area, total NH_3 emissions from these three crops were estimated at 3.01 Tg, with maize accounting for the largest share (1.32 Tg, 43.8%), followed by rice (1.21 Tg, 40.2%) and wheat (0.48 Tg, 16.0%). The dominant contribution of maize was attributable to its largest planted area and the fertilization concentrated in summer, when elevated temperatures enhance NH_3 volatilization (Yang et al., 2023; Deng et al., 2023). Our estimate was identical to the 3.01 Tg reported by Luo et al (2025), and fell within the range established by recently published inventories (Table S5). Compared with prior estimates, a key advantage of the present inventory is its daily resolution, which enables more detailed characterization of emission dynamics throughout the growing season.

NH_3 emissions from major crops in China in 2021 exhibited spatial heterogeneity in both emission factors and total emissions. Rice emission factors peaked in Guangdong at 57.80 kg ha^{-1}, 1.43 times the national mean for rice, and decreased with increasing latitude. Higher temperatures in the south accelerate urea hydrolysis and NH_3 volatilization (Yang et al., 2023; Deng et al., 2023). In addition, double-cropping rice, prevalent in the south, increases annual N inputs per unit area. Wheat emission factors increased southward across the major cropping regions from 16.36 to 23.22 kg ha^{-1}, consistent with higher temperatures and soil moisture during the fertilization period in the south. Maize emission factors generally increased southward, following the temperature gradient. The highest value was observed in Yunnan at 43.03 kg ha^{-1}, 1.41 times the national mean for maize. The higher values in Northeast China likely reflect the alkaline soils of the Songnen Plain (Chen et

https://doi.org/10.5194/egusphere-2026-6894
Preprint. Discussion started: 12 November 2026
© Author(s) 2026. CC BY 4.0 License.

al., 2019). For total emissions, hotspots were concentrated primarily in the North China Plain, the middle and lower Yangtze River Plain, and the Northeast Plain, the major production regions for the three crops, which together accounted for 67.57% of total emissions (Fig. 2d), consistent with the hotspot distribution reported by Wang et al (2025a). The dominant crop driving emissions differed by region (Fig. 2f–h). In the Northeast Plain, emissions were dominated by maize and rice. In the North China Plain, both wheat and maize were primary drivers, whereas rice dominated in the middle and lower Yangtze River Plain.



https://doi.org/10.5194/egusphere-2026-6894
Preprint. Discussion started: 12 November 2026
© Author(s) 2026. CC BY 4.0 License.

Figure 2: Spatial distribution and provincial characteristics of NH_3 emissions and emission factors for major crops in China. (a–c) Gridded NH_3 emission factor distributions for rice (a), wheat (b), and maize (c) (kg ha^{-1}). (d) Gridded NH_3 emission totals from rice, wheat, and maize (t). (e) Provincial NH_3 emissions and mean emission factors. Stacked bars show cumulative NH_3 emissions from rice, wheat, and maize (lower axis; Gg), filled circles show the mean emission factor weighted by crop area (upper axis; kg ha^{-1}). (f–h) Gridded NH_3 emission distributions for rice (f), wheat (g), and maize (h) (t).

At the provincial scale, total emissions were highest in Heilongjiang (317.56 Gg), Henan (252.77 Gg), Anhui (213.11 Gg), and Shandong (204.83 Gg), which collectively accounted for 32.83% of national emissions from the three major crops, consistent with the spatial pattern of emission hotspots in the Northeast Plain and the North China Plain (Fig. 2e). By contrast, provincial emission factors followed a contrasting spatial pattern. Emission factors were highest in South China provinces, including Guangdong (56.44 kg ha^{-1}), Hainan (54.25 kg ha^{-1}), and Guangxi (46.24 kg ha^{-1}), whereas Heilongjiang, which had the highest emissions among all provinces, recorded an emission factor of only 30.36 kg ha^{-1}. This divergence reflected the complex controls on NH_3 emissions at the regional scale. Although the rice cultivation area in Guangdong (1.83 Mha; NBS, 2022) was less than half that of Heilongjiang (3.87 Mha; NBS, 2022) the emission factor of Guangdong was 1.86 times higher. This pattern was attributable to the warm, humid climate and intensive double-cropping rice system in Guangdong, which together produced the highest provincial emission factors in China (Sheng et al., 2025; Ma et al., 2022).

3.3 Temporal Dynamics of NH_3 Emissions

3.3.1 Post-Fertilization NH_3 Volatilization Dynamics

We analyzed the mean daily variation in emission factors during the post-fertilization volatilization period (Fig. S2). In all three crops, emission factors peaked on the second day after fertilization, then declined and leveled off by the fourth day. This pattern was consistent with urea hydrolysis kinetics. Urea, the predominant nitrogen fertilizer applied to croplands in China, reaches its hydrolysis peak approximately 24–48 h after soil application, producing NH_4^+-N that is readily volatilized as NH_3 (Song et al., 2024; Shi et al., 2022; Zhao et al., 2022).

The three crops differed substantially in emission factors, despite similar temporal patterns. Rice exhibited the highest average emission factor, primarily due to flooded paddy field conditions. During daylight hours, algal photosynthesis elevates paddy floodwater pH above that of the bulk soil, thereby converting NH_4^+ to NH_3 (Li et al., 2022). In addition, rice topdressing is typically broadcast directly onto the floodwater surface, facilitating rapid NH_3 volatilization to the atmosphere. Maize exhibited the second highest emission factor, which was closely associated with the temperature conditions prevailing during its fertilization period. Maize topdressing coincided with the hot summer months (June to August), when elevated temperatures accelerated urea hydrolysis and NH_3 volatilization, resulting in higher emission factors for maize (Yang et al., 2023; Deng et al., 2023). By contrast, wheat exhibited a relatively lower emission factor.

3.3.2 Daily Variation in NH_3 Emissions

Daily analysis revealed that NH_3 emissions from major crops in China exhibited notable seasonal variation (Fig. 3a), with the annual emission peak occurring in June. Emissions were concentrated in late April to early May, early June, and late July

https://doi.org/10.5194/egusphere-2026-6894
Preprint. Discussion started: 12 November 2026
© Author(s) 2026. CC BY 4.0 License.

to early August, a multi-peak pattern reflecting overlapping emissions from multiple crops. Rice emissions peaked from April 21 to May 6 and from June 5 to 28, reaching 188.32 Gg (15.55% of annual rice emissions) and 312.56 Gg (25.80%), respectively. Maize emissions peaked from July 24 to August 10 at 445.21 Gg (33.76% of annual maize emissions), and were also high from June 1 to 13 and July 1 to 6. Wheat emissions were relatively low, concentrated primarily in April and late October, with April emissions of 227.92 Gg accounting for 47.45% of annual wheat emissions.

We statistically analyzed daily NH_3 emissions from major crops in China, excluding 43 days with zero emissions. The top 10% of days by emission magnitude (32 days) accounted for 33.11% of total annual emissions. Mean daily NH_3 emissions on these days were 31.15 Gg, 18.4 times those of the lowest 50% of days (161 days). These results indicate that NH_3 emissions were highly concentrated in a small number of days.

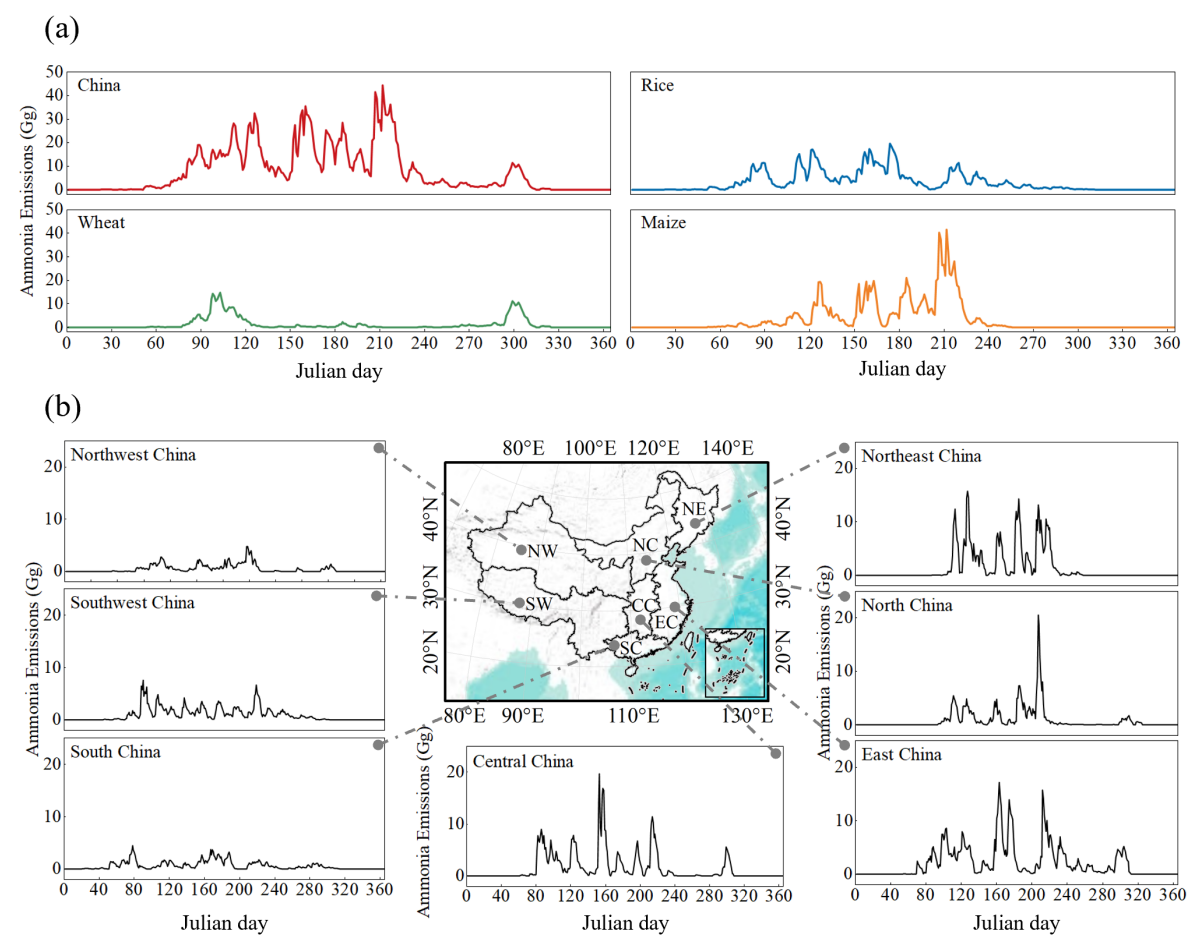


Figure 3: Temporal dynamics of NH_3 emissions in China. (a) Daily NH_3 emissions (Gg) over an annual cycle, shown for the national total and separately for rice, wheat, and maize. (b) Daily NH_3 emissions (Gg) for each of the seven geographic subregions, the central map delineates subregional boundaries.

https://doi.org/10.5194/egusphere-2026-6894
Preprint. Discussion started: 12 November 2026
© Author(s) 2026. CC BY 4.0 License.

We compared the daily emissions across seven regions of China (Fig. 3b). North China exhibited an emission pattern dominated by summer emissions, with a distinct peak in late July driven primarily by maize fertilization, which accounted for 75.52% of total regional emissions. Emissions in Northeast China reflected its single-season cropping system (Zhang et al., 2024), and were concentrated from late April to early August. During this period, fertilization events for rice and maize generated multiple closely spaced peaks of comparable intensity. East China and Central China both showed similar multi-peak emission patterns, with major peaks in early to middle June and late July to early August corresponding to the peak emission phases of rice and maize, and minor peaks in spring and autumn reflecting the wheat fertilization window. In Southwest China, emissions occurred as several smaller peaks from spring to late summer. Although South China exhibited relatively high emission factors, the limited cultivated area (NBS, 2022) prevented the formation of prominent emission peaks at the regional scale. Daily emissions appeared as multiple discrete smaller peaks throughout the growing season. Northwest China, constrained by limited water resources, arable land, and unfavorable climatic conditions (Tao et al., 2023), exhibited low annual emissions with a dispersed temporal pattern.

3.4 Accuracy and Uncertainty of Fertilization Timing

To evaluate the accuracy of the fertilization dates, we compared them against reported fertilization dates using scatter plots (Fig. 4). Quantitative evaluation showed close agreement between the identified and reported fertilization dates, with data points distributed along the 1:1 line. For basal fertilization, R was 0.95, 0.86, and 0.97 for rice, wheat, and maize, respectively. For topdressing, R reached 0.99.

https://doi.org/10.5194/egusphere-2026-6894
Preprint. Discussion started: 12 November 2026
© Author(s) 2026. CC BY 4.0 License.

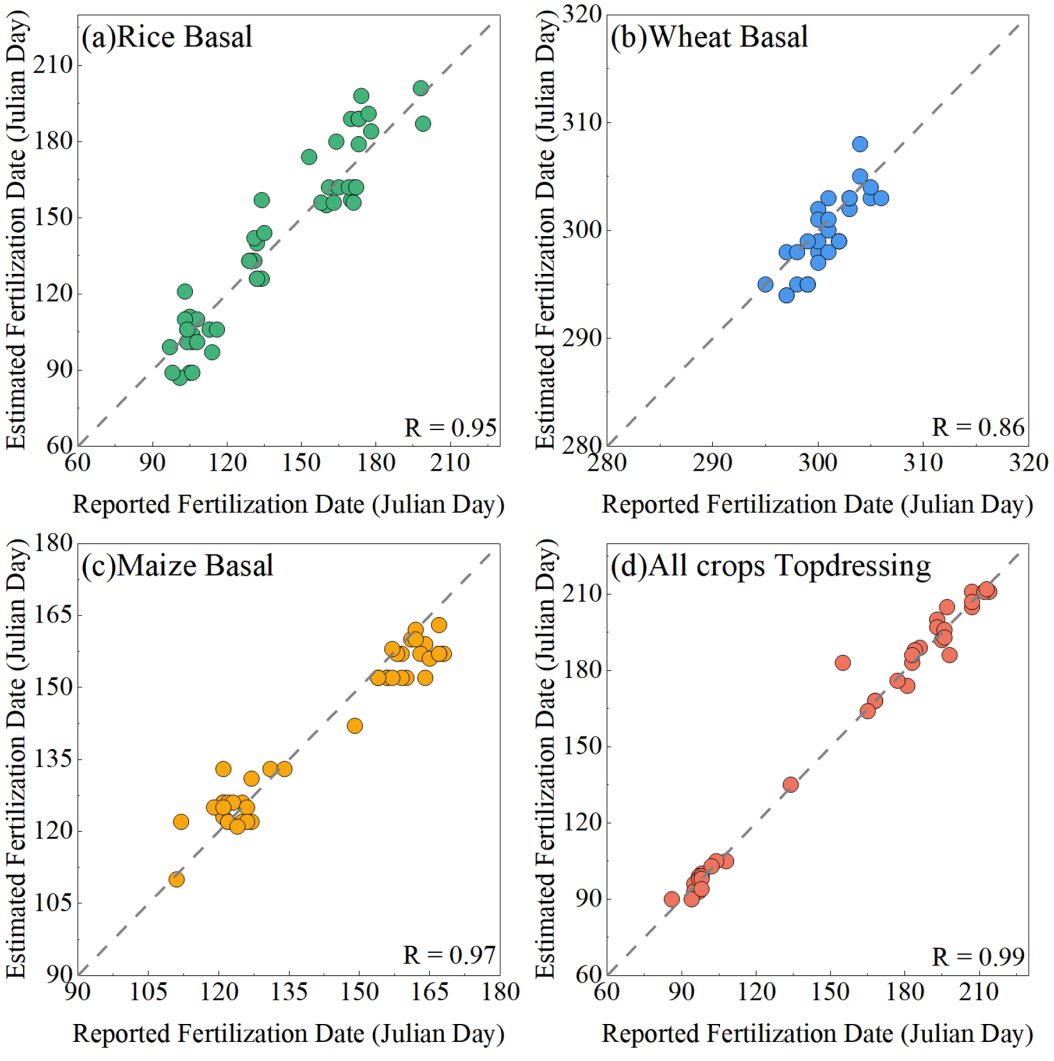
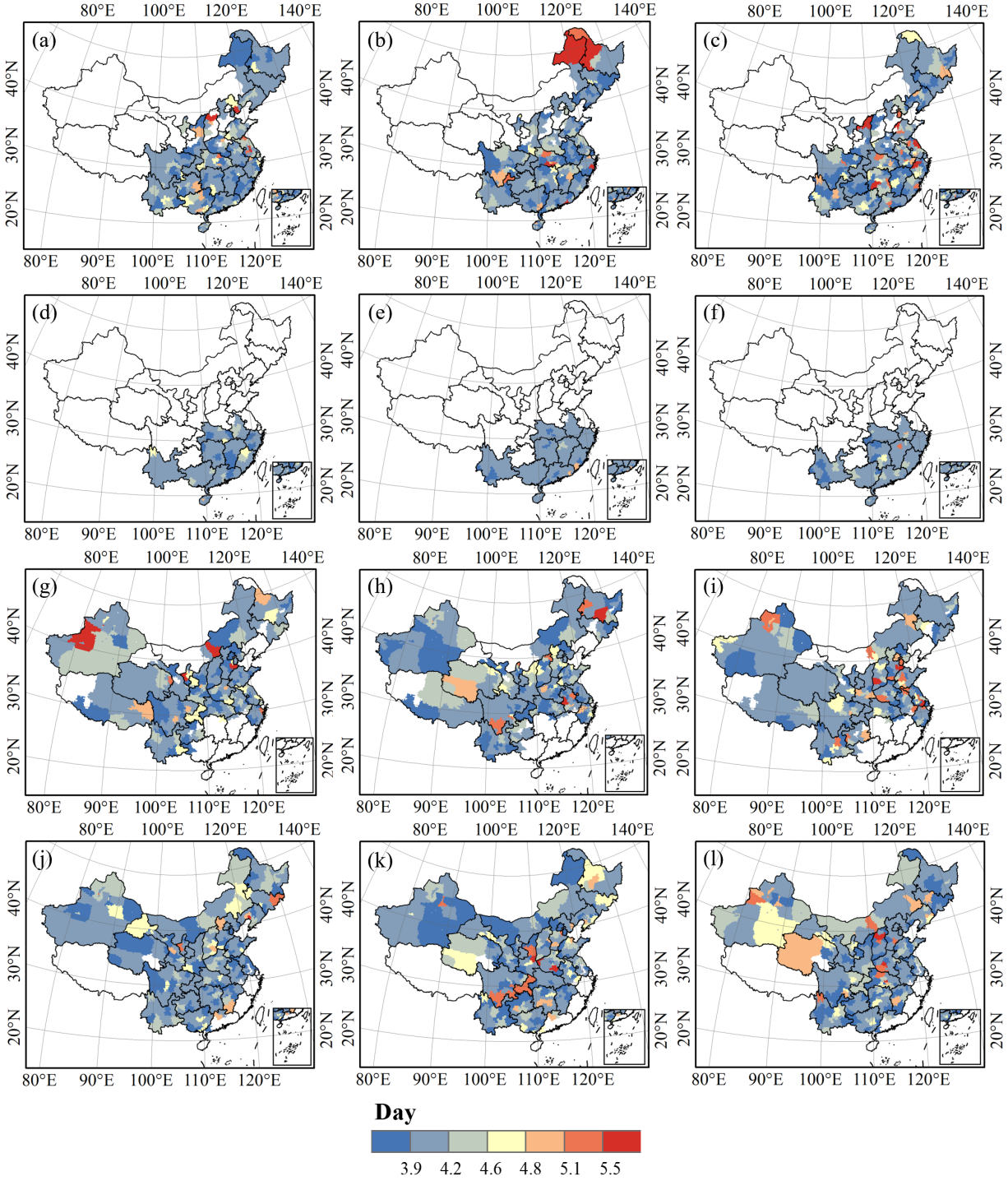


Figure 4: Scatter plots comparing reported and identified fertilization dates. (a–c) Basal fertilization for rice, wheat, and maize, respectively. (d) topdressing for the three major crops combined. Each point represents the reported and identified fertilization dates for a crop in a prefecture-level city. For rice, ERSR and LR within the same prefecture-level city are shown as separate sample points.

We further assessed the uncertainty of the fertilization dates. The mean uncertainty in fertilization dates across China was approximately ±4 days (±4.00 to 4.17 days). Spatial analysis revealed no discernible spatial pattern in uncertainty across the study domain, with neither a latitudinal gradient nor regional effects detected (Fig. 5). This absence of spatial patterning suggested that the fertilization date dataset developed in this study was free from systematic biases associated with site-specific factors. The uncertainty values for the majority of prefecture-level cities were notably concentrated in the 3.8 to 4 days interval. More than 60% of prefecture-level cities exhibited uncertainties below 4 days, and the number of cities declined sharply when uncertainty exceeded 4 days (Fig. S3).

https://doi.org/10.5194/egusphere-2026-6894
Preprint. Discussion started: 12 November 2026
© Author(s) 2026. CC BY 4.0 License.



https://doi.org/10.5194/egusphere-2026-6894
Preprint. Discussion started: 12 November 2026
© Author(s) 2026. CC BY 4.0 License.

Figure 5: Spatial distribution of uncertainty in daily fertilization timing for major crops in China. Panels (a–l) present the estimated uncertainty in fertilization dates (days) for ERSR (a–c), LR (d–f), wheat (g–i), and maize (j–l), corresponding to basal application (left column), first topdressing (middle column), and second topdressing (right column).

3.5 Daily Inventory Uncertainty and WRF-Chem Simulation Performance

3.5.1 Uncertainty in NH_3 Emission Estimates

The uncertainty in daily NH_3 emissions inventory from major crops in China in 2021 was 1.60 to 3.56 Tg in total, with crop-specific ranges of 0.65 to 1.43 Tg for rice, 0.26 to 0.57 Tg for wheat, and 0.70 to 1.56 Tg for maize. The NH_3 emission estimates reported in recently published inventories all fell within the uncertainty bounds of this study. This agreement supported the robustness of our results (Table S4). We also quantified uncertainty in NH_3 emissions and emission factors at the provincial scale. The provinces with the greatest emission uncertainty were Heilongjiang (169.63 to 375.79 Gg), Henan (135.02 to 299.12 Gg), and Anhui (113.84 to 252.20 Gg) (Fig. S4d), while those with the greatest emission factor uncertainty were Guangdong (30.15 to 66.79 kg ha^{-1}), Hainan (28.98 to 64.20 kg ha^{-1}), and Guangxi (24.70 to 54.72 kg ha^{-1}) (Fig. S4e).

3.5.2 WRF-Chem Simulations

We used WRF-Chem to simulate gridded $PM_{2.5}$ concentrations during the six pollution episodes and evaluated the results against observations. Compared with the MEIC simulations, the simulations driven by our inventory showed improved performance. Across the six episodes, R increased by 0.12 on average, and RMSE decreased by 35.34% on average (Fig. 6). The improvements were most pronounced for the three episodes in the BTH region. For the spring episode (April 17 to 25), R increased from 0.91 to 0.95, and RMSE decreased from 14.86 to 4.99, a reduction of 66.43%. For the summer episode (June 10 to 17), R increased by 0.22, from 0.73 to 0.94, and RMSE decreased from 14.28 to 11.58. For the autumn episode (October 27 to November 3), R increased from 0.69 to 0.83, and RMSE decreased from 22.24 to 20.56. For the episodes in Henan (April 4 to 12) and Guizhou (March 28 to April 7), R increased substantially from 0.71 to 0.93 and from 0.86 to 0.97, respectively. Over the same episodes, RMSE decreased from 13.51 to 8.06 and from 9.81 to 4.52, respectively. For the Jiangsu episode (October 29 to November 6), although R decreased slightly from 0.94 to 0.91, RMSE still decreased from 18.74 to 14.08, a reduction of 24.9%. Overall, these results indicate that our inventory improves the accuracy of simulated $PM_{2.5}$ dynamic.

https://doi.org/10.5194/egusphere-2026-6894
Preprint. Discussion started: 12 November 2026
© Author(s) 2026. CC BY 4.0 License.

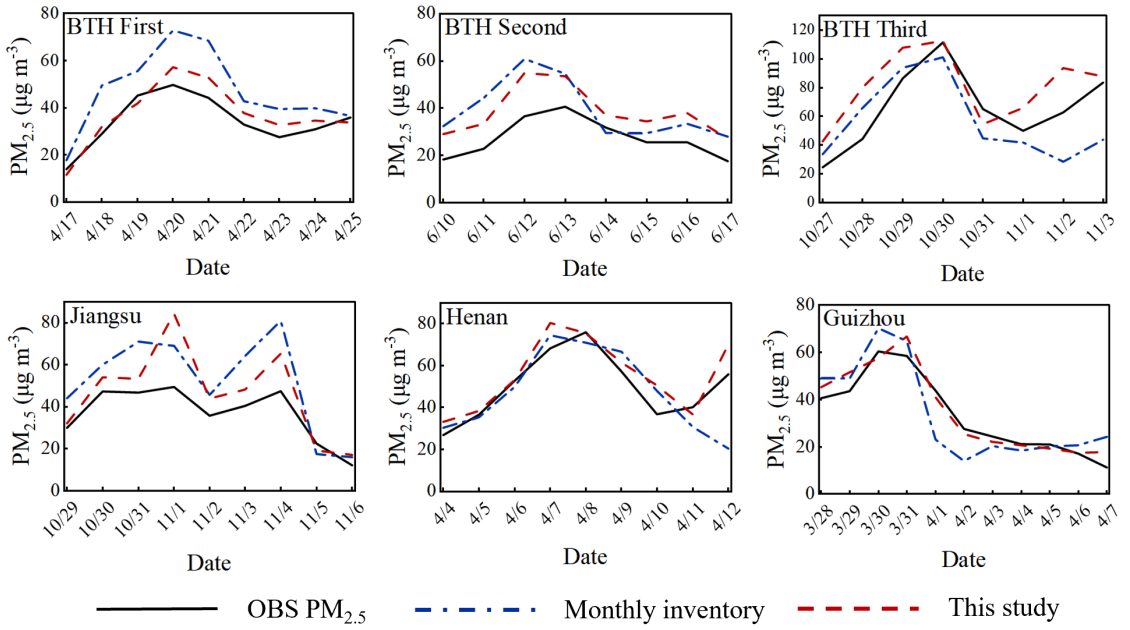


Figure 6: Time series of observed $PM_{2.5}$ concentrations and those simulated by WRF-Chem driven by different emission inventories (monthly inventory and our inventory). BTH First, BTH Second, and BTH Third denote the spring, summer, and autumn pollution episodes in the BTH region, respectively. The first day of each panel corresponds to the fertilization date. The monthly inventory developed by Zheng et al (2018, http://meicmodel.org/).

4 Conclusions

Temporal variability in $PM_{2.5}$ pollution is strongly influenced by the dynamics of NH_3 emissions, particularly their high-frequency variation driven by nitrogen fertilization. Yet few studies have resolved fertilizer-induced NH_3 emissions at a daily scale. Therefore, this study developed an innovative method that identifies daily fertilization dates from multisource satellite observations and quantifies daily NH_3 emissions using machine learning, enabling the construction of a daily emission inventory of fertilizer-induced NH_3 for China at 5 arcmin resolution. The inventory showed that total NH_3 emissions from major crop fertilization were 3.01 Tg in 2021, with maize accounting for the largest share (1.32 Tg, 43.8%), followed by rice (1.21 Tg, 40.2%) and wheat (0.48 Tg, 16.0%).

The inventory reveals pronounced spatiotemporal heterogeneity in fertilizer-induced NH_3 emissions across China. Spatially, emissions were concentrated in the North China Plain, the middle and lower Yangtze River Plain, and the Northeast Plain, which collectively contributed 67.6% of the national total. At the provincial scale, Heilongjiang had the largest total emissions (317.56 Gg), driven primarily by its extensive cropland area. By contrast, the highest emission factors occurred in southern China, reaching 56.44 kg ha^{-1} in Guangdong, attributable to the warm, humid climate and intensive double-cropping rice system. Temporally, NH_3 emissions exhibited notable seasonal variation, with the annual emission peak occurring in June. Emissions were concentrated in late April to early May, early June, and late July to early August. The top

https://doi.org/10.5194/egusphere-2026-6894
Preprint. Discussion started: 12 November 2026
© Author(s) 2026. CC BY 4.0 License.

10% of days by emission magnitude (32 days) accounted for 33.11% of total annual emissions, and mean daily emissions on these days were 31.15 Gg, 18.4 times those of the lowest 50% of days.

Our national estimate (3.01 Tg) is consistent with that reported by Luo et al (2025), and the estimates from other recently published inventories all fall within the uncertainty range of this study (1.60–3.56 Tg), which lends confidence to our results. The key advantage of the present inventory is its daily resolution. Previous studies have typically characterized fertilization timing at a monthly resolution and applied uniform fertilization windows across entire provinces, thereby neglecting substantial intra-provincial variation. The new inventory substantially improved the WRF-Chem simulation of $PM_{2.5}$. Relative to simulations driven by a conventional monthly inventory, R increased by 0.12 and RMSE decreased by 35.34% on average. These improvements suggest that the temporal misallocation of emissions in conventional monthly inventories can degrade the accuracy of $PM_{2.5}$ simulations during fertilization periods.

Two limitations of this study should be noted. The machine learning model was trained on 4,589 daily NH_3 emission records from 76 experimental sites compiled from the literature. Although this dataset includes most of the field measurements available in the literature, they still cannot fully cover all cropping regions of China, and the meteorological conditions, soil properties, and field management practices they represent may not fully capture their actual diversity across China. In addition, the WRF-Chem evaluation was conducted for the six representative pollution episodes in which the contribution of fertilizer NH_3 was pronounced, and the results showed consistent improvements. However, whether similar improvements hold for pollution episodes with more complex drivers, in which the contribution of fertilization cannot be clearly identified, and for pollution episodes in other regions requires further analysis.

The present study focused on the three major crops. To improve the accuracy and applicability, future work will extend this framework to other crops, further incorporate livestock and other agricultural sources, ultimately yielding a comprehensive agricultural NH_3 inventory at daily resolution. As air quality management in China increasingly shifts toward targeted emission controls, the daily inventory developed here could help shift mitigation from annual emission controls to interventions targeting short-term high emission episodes, potentially improving the cost-effectiveness of mitigation. In parallel, future work will expand the collection of field measurements to obtain more comprehensive training data, supporting the development of more robust models and inventories. Overall, the inventory developed in this study accurately quantifies daily NH_3 emissions from the major crops in China and provides a scientific basis for targeted agricultural emission management.

Supplement

Supplementary data and methods, supplementary results and discussion, and additional figures and tables mentioned in the text (PDF).

https://doi.org/10.5194/egusphere-2026-6894
Preprint. Discussion started: 12 November 2026
© Author(s) 2026. CC BY 4.0 License.

Author contributions

B.L. and H.L. designed the research. Y.Y. conducted the research. Y.Y., W.Z., and Y.Z. performed the model simulations. Y.Y., J.L., and W.G. contributed to data processing and the interpretation of the results. Y.Y. wrote the original manuscript. B.L. reviewed and edited the manuscript. All authors contributed to the discussion and revision of the paper.

Competing interests

The authors declare no competing financial interest.

Financial support

This work was supported by the National Natural Science Foundation of China (42377393).

References

AERIS/IASI Portal: IASI NH3R-ERA5 reanalysis product: https://iasi.aeris-data.fr/, last access: 19 October 2026.

Chen, S., Liang, Z., Webster, R., Zhang, G., Zhou, Y., Teng, H., Hu, B., Arrouays, D., and Shi, Z.: A high-resolution map of soil pH in China made by hybrid modelling of sparse soil data and environmental covariates and its implications for pollution, Sci. Total Environ., 655, 273–283, https://doi.org/10.1016/j.scitotenv.2018.11.230, 2019.

Chen, C., Xiao, W., and Chen, H. Y. H.: Mapping global soil acidification under N deposition, Glob. Change Biol., 29, 4652–4661, https://doi.org/10.1111/gcb.16813, 2023.

Chen, J., Du, X., Liu, X., Xu, W., and Krol, M.: Estimation of ammonia emissions over China using IASI satellite-derived surface observations, Environ. Sci. Technol., 59, 9991–10000, https://doi.org/10.1021/acs.est.4c10878, 2025.

China National Environmental Monitoring Centre: https://www.cnemc.cn/, last access: 19 October 2026.

Deng, X., Xu, T., Xue, L., Hou, P., Xue, L., and Yang, L.: Effects of warming and fertilization on paddy N_2O emissions and ammonia volatilization, Agr. Ecosyst. Environ., 347, 108361, https://doi.org/10.1016/j.agee.2023.108361, 2023.

Ding, J., van der A, R., Eskes, H., Dammers, E., Shephard, M., Wichink Kruit, R., Guevara, M., and Tarrason, L.: Ammonia emission estimates using CrIS satellite observations over Europe, Atmos. Chem. Phys., 24, 10583–10599, https://doi.org/10.5194/acp-24-10583-2024, 2024.

ECMWF and C3S: ERA5 reanalysis dataset: https://cds.climate.copernicus.eu/datasets, last access: 19 October 2026.

FAO and IIASA: Harmonized World Soil Database (HWSD) version 2.0: https://gaez.fao.org/pages/hwsd, last access: 19 October 2026.

Fowler, D., Coyle, M., Skiba, U., Sutton, M. A., Cape, J. N., Reis, S., Sheppard, L. J., Jenkins, A., Grizzetti, B., Galloway, J. N., Vitousek, P., Leach, A., Bouwman, A. F., Butterbach-Bahl, K., Dentener, F., Stevenson, D., Amann, M., and Voss, M.:

https://doi.org/10.5194/egusphere-2026-6894
Preprint. Discussion started: 12 November 2026
© Author(s) 2026. CC BY 4.0 License.

The global nitrogen cycle in the twenty-first century, Philos. T. R. Soc. B, 368, 20130164, https://doi.org/10.1098/rstb.2013.0164, 2013.

Geng, G., Zheng, Y., Zhang, Q., Xue, T., Zhao, H., Tong, D., Zheng, B., Li, M., Liu, F., Hong, C., He, K., and Davis, S. J.: Drivers of $PM_{2.5}$ air pollution deaths in China 2002–2017, Nat. Geosci., 14, 645–650, https://doi.org/10.1038/s41561-021-00792-3, 2021.

Huang, X., Song, Y., Li, M., Li, J., Huo, Q., Cai, X., Zhu, T., Hu, M., and Zhang, H.: A high-resolution ammonia emission inventory in China, Global Biogeochem. Cy., 26, GB1030, https://doi.org/10.1029/2011GB004161, 2012.

Joseph, L. P., Deo, R. C., Prasad, R., Salcedo-Sanz, S., Raj, N., and Soar, J.: Near real-time wind speed forecast model with bidirectional LSTM networks, Renew. Energ., 204, 39–58, https://doi.org/10.1016/j.renene.2022.12.123, 2023.

Kang, Y., Liu, M., Song, Y., Huang, X., Yao, H., Cai, X., Zhang, H., Kang, L., Liu, X., Yan, X., He, H., Zhang, Q., Shao, M., and Zhu, T.: High-resolution ammonia emissions inventories in China from 1980 to 2012, Atmos. Chem. Phys., 16, 2043–2058, https://doi.org/10.5194/acp-16-2043-2016, 2016.

Kuang, Y., Xu, W., Lin, W., Meng, Z., Zhao, H., Ren, S., Zhang, G., Liang, L., and Xu, X.: Explosive morning growth phenomena of NH_3 on the North China Plain: causes and potential impacts on aerosol formation, Environ. Pollut., 257, 113621, https://doi.org/10.1016/j.envpol.2019.113621, 2020.

Li, B., Chen, L., Shen, W., Jin, J., Wang, T., Wang, P., Yang, Y., and Liao, H.: Improved gridded ammonia emission inventory in China, Atmos. Chem. Phys., 21, 15883–15900, https://doi.org/10.5194/acp-21-15883-2021, 2021.

Li, S., Zhang, W., Zheng, X., Li, Y., Han, S., Wang, R., Wang, K., Yao, Z., Liu, C., and Zhang, C.: Update of a biogeochemical model with process-based algorithms to predict ammonia volatilization from fertilized cultivated uplands and rice paddy fields, Biogeosciences, 19, 3001–3019, https://doi.org/10.5194/bg-19-3001-2022, 2022.

Li, B., Liao, H., Li, K., Wang, Y., Zhang, L., Guo, Y., Liu, L., Li, J., Jin, J., Yang, Y., Gong, C., Wang, T., Shen, W., Wang, P., Dang, R., Liao, K., Zhu, Q., and Jacob, D. J.: Unlocking nitrogen management potential via large-scale farming for air quality and substantial co-benefits, Natl. Sci. Rev., 11, nwae324, https://doi.org/10.1093/nsr/nwae324, 2024.

Li, B., Liao, H., Li, K., Lin, J., Gong, C., Liu, H., Li, Y., Chen, L., Yang, Y., Jin, X., Zhao, Y., Wang, T., Jin, J., Dang, R., and Jacob, D. J.: Environmental burden and health inequity in China's road-based express delivery, Nat. Cities, 2, 825–834, https://doi.org/10.1038/s44284-025-00300-3, 2025.

Liu, L., Xu, W., Lu, X., Zhong, B., Guo, Y., Lu, X., Zhao, Y., He, W., Wang, S., Zhang, X., Liu, X., and Vitousek, P.: Exploring global changes in agricultural ammonia emissions and their contribution to nitrogen deposition since 1980, P. Natl. Acad. Sci. USA, 119, e2121998119, https://doi.org/10.1073/pnas.2121998119, 2022a.

Liu, P., Ding, J., Liu, L., Xu, W., and Liu, X.: Estimation of surface ammonia concentrations and emissions in China from the polar-orbiting Infrared Atmospheric Sounding Interferometer and the FY-4A Geostationary Interferometric Infrared Sounder, Atmos. Chem. Phys., 22, 9099–9110, https://doi.org/10.5194/acp-22-9099-2022, 2022b.

https://doi.org/10.5194/egusphere-2026-6894
Preprint. Discussion started: 12 November 2026
© Author(s) 2026. CC BY 4.0 License.

Liu, J., Li, B., Zhu, Q., Zhao, Y., Wang, T., Liao, K., Li, Y., Gu, W., Zhang, W., and Liao, H.: Ammonia transfers through interprovincial agricultural trade and their health burden implications in China, Environ. Res. Lett., 20, 084077, https://doi.org/10.1088/1748-9326/adf12a, 2025.

Luo, Y., Zhang, Z., Chen, Y., Li, Z., and Tao, F.: ChinaCropPhen1km: a high-resolution crop phenological dataset for three staple crops in China during 2000–2015 based on leaf area index (LAI) products, Earth Syst. Sci. Data, 12, 197–214, https://doi.org/10.5194/essd-12-197-2020, 2020.

Luo, B., Liu, L., Yung, D. H. Y., Yuan, T., Zhang, J., Ng, L. T. H., and Tai, A. P. K.: Effects of enhancing nitrogen use efficiency in cropland and livestock systems on agricultural ammonia emissions and particulate matter air quality in China, Atmos. Chem. Phys., 25, 10089–10108, https://doi.org/10.5194/acp-25-10089-2025, 2025.

Lyu, Y., Ju, Q., Lv, F., Feng, J., Pang, X., and Li, X.: Spatiotemporal variations of air pollutants and ozone prediction using machine learning algorithms in the Beijing-Tianjin-Hebei region from 2014 to 2021, Environ. Pollut., 306, 119420, https://doi.org/10.1016/j.envpol.2022.119420, 2022.

Ma, R., Yu, K., Xiao, S., Liu, S., Ciais, P., and Zou, J.: Data-driven estimates of fertilizer-induced soil NH_3, NO and N_2O emissions from croplands in China and their climate change impacts, Glob. Change Biol., 28, 1008–1022, https://doi.org/10.1111/gcb.15975, 2022.

Miinalainen, T., Kokkola, H., Lipponen, A., Hyvärinen, A.-P., Soni, V. K., Lehtinen, K. E. J., and Kühn, T.: Assessing the climate and air quality effects of future aerosol mitigation in India using a global climate model combined with statistical downscaling, Atmos. Chem. Phys., 23, 3471–3491, https://doi.org/10.5194/acp-23-3471-2023, 2023.

Minoli, S., Jägermeyr, J., Asseng, S., Urfels, A., and Müller, C.: Global crop yields can be lifted by timely adaptation of growing periods to climate change, Nat. Commun., 13, 7079, https://doi.org/10.1038/s41467-022-34411-5, 2022.

National Bureau of Statistics of China: China Statistical Yearbook 2022, China Statistics Press, Beijing, ISBN 9787503799501, 2022.

National Development and Reform Commission Price Department and Cost Survey Center: National Agricultural Product Cost and Income Data Compilation 2022, China Statistics Press, Beijing, ISBN 9787503799723, 2022.

Qiao, X., Ying, Q., Li, X., Zhang, H., Hu, J., Tang, Y., and Chen, X.: Source apportionment of $PM_{2.5}$ for 25 Chinese provincial capitals and municipalities using a source-oriented Community Multiscale Air Quality model, Sci. Total Environ., 612, 462–471, https://doi.org/10.1016/j.scitotenv.2017.08.272, 2018.

Qiu, B., Wu, F., Hu, X., Yang, P., Wu, W., Chen, J., Chen, X., He, L., Joe, B., Tubiello, F. N., Qian, J., and Wang, L.: A robust framework for mapping complex cropping patterns: the first national-scale 10 m map with 10 crops in China using Sentinel 1/2 images, ISPRS J. Photogramm., 224, 361–381, https://doi.org/10.1016/j.isprsjprs.2025.04.012, 2025.

Ren, C., Huang, X., Liu, T., Song, Y., Wen, Z., Liu, X., Ding, A., and Zhu, T.: A dynamic ammonia emission model and the online coupling with WRF–Chem (WRF–SoilN–Chem v1.0): development and regional evaluation in China, Geosci. Model Dev., 16, 1641–1659, https://doi.org/10.5194/gmd-16-1641-2023, 2023.

https://doi.org/10.5194/egusphere-2026-6894
Preprint. Discussion started: 12 November 2026
© Author(s) 2026. CC BY 4.0 License.

Ren, C., Huang, X., Wang, Y., Zhang, L., Zhou, X., Sun, W., Zhang, H., Liu, T., Ding, A., and Wang, T.: Enhanced soil emissions of reactive nitrogen gases by fertilization and their impacts on secondary air pollution in eastern China, Environ. Sci. Technol., 59, 5119–5130, https://doi.org/10.1021/acs.est.4c12324, 2025a.

Ren, T., Miao, T., Li, X., Zhang, W., Smreczak, B., Ukalska-Jaruga, A., Li, Y., and Cai, A.: Global pattern and drivers of soil soluble organic nitrogen, Innovation Geosci., 3, 100151, https://doi.org/10.59717/j.xinn-geo.2025.100151, 2025b.

Shen, Q., Tang, B., Wu, X., Kang, J., Li, J., Pan, Y., Liu, X., and Xu, W.: A large net source revealed by the atmospheric reactive nitrogen budget in a subtropical plateau lake basin, southwest China, Nitrogen Cycl., 2, e006, https://doi.org/10.48130/nc-0025-0018, 2026.

Sheng, L., Guo, Y., Wu, Y., Huang, Z., Yuan, X., Zhu, K., Wu, L., Zhang, J., Wang, Z., Huang, Y., Zhong, Z., Zhang, T., Chen, D., Wang, B., and Zheng, J.: Evaluation and diagnosis of regional ammonia emission inventory in the Pearl River Delta using multisite NH_3 observations and model simulations, Environ. Sci. Technol., 59, 19318–19329, https://doi.org/10.1021/acs.est.5c01380, 2025.

Shephard, M. W., Dammers, E., Cady-Pereira, K. E., Kharol, S. K., Thompson, J., Gainariu-Matz, Y., Zhang, J., McLinden, C. A., Kovachik, A., Moran, M., Bittman, S., Sioris, C. E., Griffin, D., Alvarado, M. J., Lonsdale, C., Savic-Jovcic, V., and Zheng, Q.: Ammonia measurements from space with the Cross-track Infrared Sounder: characteristics and applications, Atmos. Chem. Phys., 20, 2277–2302, https://doi.org/10.5194/acp-20-2277-2020, 2020.

Shi, X., Li, X., Guo, C., Feng, P., and Hu, K.: Modeling ammonia volatilization following urea and controlled-release urea application to paddy fields, Comput. Electron. Agr., 196, 106888, https://doi.org/10.1016/j.compag.2022.106888, 2022.

Song, L., Wang, A., Li, Z., Kang, R., Walters, W. W., Pan, Y., Quan, Z., Huang, S., and Fang, Y.: Large seasonal variation in nitrogen isotopic abundances of ammonia volatilized from a cropland ecosystem and implications for regional NH_3 source partitioning, Environ. Sci. Technol., 58, 1177–1186, https://doi.org/10.1021/acs.est.3c08800, 2024.

Tao, W., Deng, M., Wang, Q., Su, L., Ma, C., and Ning, S.: Ecological agriculture connotation and pathway of high-quality agricultural development system in northwest arid region, T. Chin. Soc. Agr. Eng., 39, 221–232, https://doi.org/10.11975/j.issn.1002-6819.202305240, 2023.

Multi-resolution Emission Inventory model for Climate and air pollution research (MEIC): http://meicmodel.org/, last access: 19 October 2026.

Van Damme, M., Clarisse, L., Heald, C. L., Hurtmans, D., Ngadi, Y., Clerbaux, C., Dolman, A. J., Erisman, J. W., and Coheur, P. F.: Global distributions, time series and error characterization of atmospheric ammonia (NH_3) from IASI satellite observations, Atmos. Chem. Phys., 14, 2905–2922, https://doi.org/10.5194/acp-14-2905-2014, 2014.

Wang, C., Cheng, K., Ren, C., Liu, H., Sun, J., Reis, S., Yin, S., Xu, J., and Gu, B.: An empirical model to estimate ammonia emission from cropland fertilization in China, Environ. Pollut., 288, 117982, https://doi.org/10.1016/j.envpol.2021.117982, 2021a.

https://doi.org/10.5194/egusphere-2026-6894
Preprint. Discussion started: 12 November 2026
© Author(s) 2026. CC BY 4.0 License.

Wang, Y., Fu, X., Wu, D., Wang, M., Lu, K., Mu, Y., Liu, Z., Zhang, Y., and Wang, T.: Agricultural fertilization aggravates air pollution by stimulating soil nitrous acid emissions at high soil moisture, Environ. Sci. Technol., 55, 14556–14566, https://doi.org/10.1021/acs.est.1c04134, 2021b.

Wang, C., Liu, Z., Zhang, X., Zhang, L., Zhou, F., Ti, C., Adalibieke, W., Peng, L., Zhan, X., Reis, S., Liu, H., Zhu, Z., Dong, H., Xu, J., and Gu, B.: Managing ammonia for multiple benefits based on verified high-resolution emission inventory in China, Environ. Sci. Technol., 59, 5131–5144, https://doi.org/10.1021/acs.est.4c12558, 2025a.

Wang, L., Du, H., Zhang, Z., Hu, G., Mirjalili, S., Khodadadi, N., Hussien, A. G., Liao, Y., and Zhao, W.: Tianji's Horse Racing Optimization (THRO): a new metaheuristic inspired by ancient wisdom and its engineering optimization applications, Artif. Intell. Rev., 58, 282, https://doi.org/10.1007/s10462-025-11269-9, 2025b.

Wolkovich, E. M., Cook, B. I., Allen, J. M., Crimmins, T. M., Betancourt, J. L., Travers, S. E., Pau, S., Regetz, J., Davies, T. J., Kraft, N. J. B., Ault, T. R., Bolmgren, K., Mazer, S. J., McCabe, G. J., McGill, B. J., Parmesan, C., Salamin, N., Schwartz, M. D., and Cleland, E. E.: Warming experiments underpredict plant phenological responses to climate change, Nature, 485, 494–497, https://doi.org/10.1038/nature11014, 2012.

Wu, H., Li, Y., Xie, Z., Sun, J., Smith, P., Cheng, K., Fan, P., Yue, Q., and Pan, G.: Estimating ammonia emissions from cropland in China based on the establishment of agro-region-specific models, Agr. Forest Meteorol., 303, 108373, https://doi.org/10.1016/j.agrformet.2021.108373, 2021.

Wu, C., He, H., Song, R., Zhu, X., Peng, Z., Fu, Q., and Pan, J.: A hybrid deep learning model for regional O_3 and NO_2 concentrations prediction based on spatiotemporal dependencies in air quality monitoring network, Environ. Pollut., 320, 121075, https://doi.org/10.1016/j.envpol.2023.121075, 2023.

Wu, N., Geng, G., Xu, R., Liu, S., Liu, X., Shi, Q., Zhou, Y., Zhao, Y., Liu, H., Song, Y., Zheng, J., Zhang, Q., and He, K.: Development of a high-resolution integrated emission inventory of air pollutants for China, Earth Syst. Sci. Data, 16, 2893–2915, https://doi.org/10.5194/essd-16-2893-2024, 2024.

Xia, J., Zhou, Y., Fang, L., Qi, Y., Li, D., Liao, H., and Jin, J.: South Asia anthropogenic ammonia emission inversion through assimilating IASI observations, Atmos. Chem. Phys., 25, 7071–7086, https://doi.org/10.5194/acp-25-7071-2025, 2025.

Xu, W., Liu, X., Liu, L., Dore, A. J., Tang, A., Lu, L., Wu, Q., Zhang, Y., Hao, T., Pan, Y., Chen, J., and Zhang, F.: Impact of emission controls on air quality in Beijing during APEC 2014: implications from water-soluble ions and carbonaceous aerosol in $PM_{2.5}$ and their precursors, Atmos. Environ., 210, 241–252, https://doi.org/10.1016/j.atmosenv.2019.04.050, 2019.

Xu, X., Ouyang, X., Gu, Y., Cheng, K., Smith, P., Sun, J., Li, Y., and Pan, G.: Climate change may interact with nitrogen fertilizer management leading to different ammonia loss in China's croplands, Glob. Change Biol., 27, 6525–6535, https://doi.org/10.1111/gcb.15874, 2021.

Yang, W., Que, H., Wang, S., Zhu, A., Zhang, Y., He, Y., Xin, X., Zhang, X., and Ding, S.: High temporal resolution measurements of ammonia emissions following different nitrogen application rates from a rice field in the Taihu Lake region of China, Environ. Pollut., 257, 113489, https://doi.org/10.1016/j.envpol.2019.113489, 2020.

https://doi.org/10.5194/egusphere-2026-6894
Preprint. Discussion started: 12 November 2026
© Author(s) 2026. CC BY 4.0 License.

Yang, W., Hu, Y., Song, C., Yu, Y., and Jiao, Y.: Interactive effects of soil moisture, nitrogen fertilizer, and temperature on the kinetic and thermodynamic properties of ammonia emissions from alkaline soil, Atmos. Pollut. Res., 14, 101805, https://doi.org/10.1016/j.apr.2023.101805, 2023.

Ye, Z., Li, J., Pan, Y., Wang, Z., Guo, X., Cheng, L., Tang, X., Zhu, J., Kong, L., Song, Y., Xing, J., Sun, Y., and Pan, X.: Synergistic effect of reductions in multiple gaseous precursors on secondary inorganic aerosols in winter under a meteorology-based redistributed daily NH_3 emission inventory within the Beijing-Tianjin-Hebei region, China, Sci. Total Environ., 821, 153383, https://doi.org/10.1016/j.scitotenv.2022.153383, 2022.

Yin, J., Deng, Z., Ines, A. V. M., Wu, J., and Rasu, E.: Forecast of short-term daily reference evapotranspiration under limited meteorological variables using a hybrid bi-directional long short-term memory model (Bi-LSTM), Agr. Water Manage., 242, 106386, https://doi.org/10.1016/j.agwat.2020.106386, 2020.

Zhan, X., Bo, Y., Zhou, F., Liu, X., Paerl, H. W., Shen, J., Wang, R., Li, F., Tao, S., Dong, Y., and Tang, X.: Evidence for the importance of atmospheric nitrogen deposition to eutrophic Lake Dianchi, China, Environ. Sci. Technol., 51, 6699–6708, https://doi.org/10.1021/acs.est.6b06135, 2017.

Zhan, X., Adalibieke, W., Cui, X., Winiwarter, W., Reis, S., Zhang, L., Bai, Z., Wang, Q., Huang, W., and Zhou, F.: Improved estimates of ammonia emissions from global croplands, Environ. Sci. Technol., 55, 1329–1338, https://doi.org/10.1021/acs.est.0c05149, 2021.

Zhang, L., Chen, Y., Zhao, Y., Henze, D. K., Zhu, L., Song, Y., Paulot, F., Liu, X., Pan, Y., Lin, Y., and Huang, B.: Agricultural ammonia emissions in China: reconciling bottom-up and top-down estimates, Atmos. Chem. Phys., 18, 339–355, https://doi.org/10.5194/acp-18-339-2018, 2018.

Zhang, Q., Zheng, Y., Tong, D., Shao, M., Wang, S., Zhang, Y., Xu, X., Wang, J., He, H., Liu, W., Ding, Y., Lei, Y., Li, J., Wang, Z., Zhang, X., Wang, Y., Cheng, J., Liu, Y., Shi, Q., Yan, L., Geng, G., Hong, C., Li, M., Liu, F., Zheng, B., Cao, J., Ding, A., Gao, J., Fu, Q., Huo, J., Liu, B., Liu, Z., Yang, F., He, K., and Hao, J.: Drivers of improved $PM_{2.5}$ air quality in China from 2013 to 2017, P. Natl. Acad. Sci. USA, 116, 24463–24469, https://doi.org/10.1073/pnas.1907956116, 2019.

Zhang, S., Shen, G., Yu, Q., and Wu, W.: Remote sensing detection of cropping system and its spatial-temporal pattern in China, Sci. Agr. Sin., 57, 1469–1489, https://doi.org/10.3864/j.issn.0578-1752.2024.08.005, 2024.

Zhang, W., Li, B., Liu, J., Gu, W., Li, Y., Liao, K., and Zhu, Q.: High-resolution livestock spatial distribution mapping in China based on big data and applications in ammonia emission inventories, J. Clean. Prod., 520, 146097, https://doi.org/10.1016/j.jclepro.2025.146097, 2025.

Zhao, R., Liu, J., Xu, N., He, T., Meng, J., and Liu, Z.: Urea hydrolysis in different farmland soils as affected by long-term biochar application, Front. Environ. Sci., 10, 950482, https://doi.org/10.3389/fenvs.2022.950482, 2022.

Zhao, Y., Li, B., Dong, J., Li, Y., Wang, X., Gan, C., Lin, Y., and Liao, H.: Improved ammonia emission inventory of fertilizer application for three major crops in China based on phenological data, Sci. Total Environ., 896, 165225, https://doi.org/10.1016/j.scitotenv.2023.165225, 2023.

https://doi.org/10.5194/egusphere-2026-6894
Preprint. Discussion started: 12 November 2026
© Author(s) 2026. CC BY 4.0 License.



Zheng, B., Tong, D., Li, M., Liu, F., Hong, C., Geng, G., Li, H., Li, X., Peng, L., Qi, J., Yan, L., Zhang, Y., Zhao, H., Zheng, Y., He, K., and Zhang, Q.: Trends in China's anthropogenic emissions since 2010 as the consequence of clean air actions, Atmos. Chem. Phys., 18, 14095–14111, https://doi.org/10.5194/acp-18-14095-2018, 2018.

Zhou, F., Ciais, P., Hayashi, K., Galloway, J., Kim, D., Yang, C., Li, S., Liu, B., Shang, Z., and Gao, S.: Re-estimating NH_3 emissions from Chinese cropland by a new nonlinear model, Environ. Sci. Technol., 50, 564–572, https://doi.org/10.1021/acs.est.5b03156, 2016.